Suction power output and the inertial cost of rotating the neurocranium to generate suction in fish

Sam Van Wassenbergh[a,b,*], Steven W. Day[c], L. Patricia Hernández[d], Timothy E. Higham[e], Tyler Skorczewski[f,g]

[a]Department of Biology, Ghent University, K. L. Ledeganckstraat 35, B-9000 Gent, Belgium
[b]Department of Biology, University of Antwerp, Universiteitsplein 1, B-2610 Antwerpen, Belgium
[c]Department of Mechanical Engineering, Rochester Institute of Technology, 76 Lomb Memorial Dr., Rochester, NY 14623 USA
[d]Department of Biological Sciences, Lisner Hall Rm 340, The George Washington University, 2023 G St NW, Washington, DC 20052, USA
[e]Department of Biology, University of California, 900 University Avenue, Riverside, California, USA 92521
[f]Department of Mathematics, University of Utah, 155 S 1400 E, Salt Lake City, Utah, USA
[g]Department of Mathematics and Statistics, Cornell College, 600 First Street SW, Mount Vernon, Iowa, USA

*****Corresponding author at: Department of Biology, Ghent University, K. L. Ledeganckstraat 35, B-9000 Gent, Belgium
e-mail: sam.vanwassenbergh@ugent.be
Tel: +32 9 264.52.33
Fax: +32 9 264.53.44

Highlights

- Neurocranial rotation dynamics of fish is described by an inverse dynamic model.
- The inertial cost of accelerating the neurocranium is small in largemouth bass.
- Kinetic energy of the neurocranium is probably converted into suction work.
- Suction performance is not limited by cranial mass in generalized percomorph fish.

Abstract

To expand the buccal cavity, many suction-feeding fishes rely on a considerable contribution from dorsal rotation of the dorsal part of the head including the brains, eyes, and several bones forming the braincase and skull roof (jointly referred to as the neurocranium). As the neurocranium takes up a large part of the total mass of the head, this rotation may incur a considerable inertial cost. If so, this would suggest a significant selective pressure on the kinematics and mass distribution of the neurocranium of suction feeders. Here, an inverse dynamic model is formulated to calculate the instantaneous power required to rotate the neurocranium, approximated by a quarter ellipsoid volume of homogeneous density, as well as to calculate the instantaneous suction power based on intra-oral pressure and head volume quantifications. We applied this model to largemouth bass (*Micropterus salmoides*) and found that the power required to rotate the neurocranium accounts for only about 4% of the power required to suck water into the mouth. Furthermore, recovery of kinetic energy from the rotating neurocranium converted into suction work may be possible during the phase of neurocranial deceleration. Thus, we suggest that only a negligible proportion of the power output of the feeding muscles is lost as inertial costs in the largemouth bass. Consequently, the feeding performance of piscivorous suction feeders with generalised morphology, comparable to our model species, is not limited by neurocranial motion during head

expansion. This suggests that it is thus not likely to be a factor of importance in the evolution of cranial shape and size.

Key Words: biomechanics, inverse dynamics, prey capture, cranium

1. Introduction

Many aquatic vertebrates rely on generating a flow of water from the external environment into the mouth to capture prey (e.g., Lauder and Schaffen, 1993). Conservation of mass and the incompressibility of water dictate that any expansion of the buccopharyngeal cavity will generate a flow of water. During this process, which is typically referred to as suction feeding, prey items situated in the flow field in front of the mouth will experience hydrodynamic forces (Holzman et al., 2007; Skorczewski et al., 2010; Wainwright and Day, 2006). These forces are associated with highly unsteady water flows: adult suction feeders generally manage to accelerate water and prey from standstill to over 1 m s^{-1} in less than 0.05 s (Higham et al., 2006a; van Leeuwen, 1984; Van Wassenbergh et al., 2007a). In order to maximize suction feeding success on prey adhering to the substrate or trying to escape, the sudden increase in flow velocity in front of the mouth must be maximized. In other words, suction feeders must transfer as much kinetic energy to the water in the shortest possible amount of time. Consequently, to maximise prey capture performance, suction feeders must maximise instantaneous power.

To generate this power, fish mainly rely on contraction of the voluminous post-cranial musculature (Aerts, 1991; Camp and Brainerd, 2014; Carroll and Wainwright, 2006; Coughlin and Carroll, 2006; Muller, 1987; Thys, 1997; Van Wassenbergh et al., 2007b). This musculature consists of hypaxial (ventral to the vertebral column) and epaxial (dorsal to the vertebral column) components (Fig. 1A). Contraction of the hypaxial musles rotates the pectoral girdle posteriorly, while contraction of the epaxial muscles induce a dorsal rotation

of the neurocranium (Fig. 1B). Despite rotating different skeletal elements, the role of hypaxial and epaxial muscle contractions in suction generation is identical: they both increase the angle between the pectoral girdle and the neurocranium, which in turn causes a displacement of the "roof" and the "floor" of the mouth cavity away from each other. This separation increases the buccopharyngeal volume. The increased angle between pectoral girdle and neurocranium results in an additional complex sequence of coupled motions of the hyoid arch and lower jaw which push on the ventral side of the mouth cavity tissues, and which via the hyoid also enforce widening of the head by suspensorium abduction (Aerts, 1991; De Visser and Barel, 1996; Muller, 1989). Although relatively small cranial muscles such as the *sternohyoideus*, *protractor hyoideus*, *levator arcus palatini*, and *levator operculi* probably assist in powering suction (e.g., Osse, 1968), their cumulative mass, and thus potential contribution to power generation, is small compared to the hypaxials and/or epaxials (Carroll and Wainwright, 2009).

Not all power produced by the feeding musculature will result in water acceleration: an unknown amount of the muscle's power output will be lost due to the musculoskeletal mechanics underlying suction generation. Examples are joint friction, stretching of skin, resistive stress in the adductor muscles (e.g. *adductor mandibulae* during mouth opening), hydrodynamic resistance at the external head surfaces, and the inertia of the elements involved in expanding the buccopharygeal cavity. A study on suction feeding of the catfish *Clarias gariepinus* estimated that inertial force (integral over the entire buccopharyngeal cavity of acceleration multiplied by mass of the displaced tissues) is about 10% of the pressure force on the buccopharyngeal cavity surfaces (Van Wassenbergh et al., 2005). However, as *C. gariepinus* relies almost entirely on ventral depressions of the floor of the mouth cavity to generate suction, *C. gariepinus* is atypical compared to many other suction

feeders (Gibb and Ferry-Graham, 2005) in showing (on average) no rotation of the neurocranium.

Dorsorotation of a large neurocranial mass for generating buccopharyngeal expansion may require an important fraction of the power budget of suction feeding. Of the potential sources of power loss identified above, it is the most conspicuous candidate as it is both massive and experiences large accelerations. In adult fishes, the functional unit referred to here as "neurocranium" typically includes a strongly ossified protective braincase and the brain, the eyes surrounded by the circumorbital bones, and anterior bony elements such as the rostrum, ethmoid, and vomer. During suction feeding, the neurocranium is rotated along with the suspensoria, upper oral and pharyngeal jaws attached to it. Measurements of *Micropterus salmoides* (*largemouth bass*), for example, show that the mass of this functional unit equals approximately 60% of the total cranium (including sternohyoideus and cleithrum).

Given the importance of feeding success for survival, a considerable inertial cost to rotate the neurocranium would imply a significant selective pressure on the shape and size of the neurocranium (or more specifically on the pitching moment of inertia about the instantaneous center of neurocranial rotation). Alternatively, recruitment of only the relatively light-weight, ventro-lateral series of skeletal elements by the hypaxial muscles for generating suction power would probably be favoured in case evolution has resulted in a neurocranium that is too heavy to retain a reasonable power efficiency (e.g. inertial losses divided by hydrodynamic power output). Unfortunately, the relative importance of the inertial cost of neurocranial elevation is currently unknown. Yet, this mechanical insight seems essential to better understand the functional morphology and kinematics of suction feeding fish.

To determine to what extent inertial costs of rotating the neurocranium affect suction performance, we address the following aims: (1) formulate an inverse dynamic model for

estimating the instantaneous power requirement for rotating the neurocranium as observed on lateral-view high-speed videos, (2) establish a theoretical framework and mathematical models for calculating the total hydrodynamic power of suction feeding from different sources of experimental data and model simulations, (3) evaluate the results of these models for suction feeding in a species with a generalized percomorph trophic habit (*Micropterus salmoides*).

2. Methods

2.1 Inverse dynamic model of neurocranial rotation

To calculate the inertial power required to rotate the neurocranium, the following mathematical model is used. The shape of the neurocranium is modeled as a quarter of an ellipsoid. This shape is chosen since elliptical cross-sections have proven to fit the external contours of fish relatively accurately (Drost and van den Boogaart, 1986), and ellipsoids can capture the anterior narrowing of a streamlined head. By setting l (length), h (height) and w (width) as the dimensions of the neurocranium (Fig. 2), the volume (V) of the quarter ellipsoid model of the neurocranium is

$$V = \frac{1}{4}\frac{4}{3}\pi l h \frac{w}{2} = \frac{1}{6}\pi l h w \quad (1).$$

Assuming a uniform density (ρ) of the tissues filling this quarter ellipsoid, its mass (m) equals

$$m = \frac{1}{6}\pi l h w \rho \quad (2).$$

Assigning the origin of an orthogonal coordinate frame to the center of the full ellipsoid (x-axis = posterior-anterior; y-axis = ventral-dorsal; z-axis = left-right; Fig. 2) results in a location of the center of mass (COM) of the quarter ellipsoid at point ($3l/8$, $3h/8$, 0). The

moment of inertia for rotation about the *z*-axis through the origin of this coordinate frame (i.e., pitching about the base corner of the quarter ellipsoid) can be derived (e.g. Landau and Lifshitz, 1976):

$$I_{origin} = \frac{\rho l h w \pi}{30}(l^2 + h^2) \quad (3).$$

Using the parallel axis theorem we have the following result:

$$I_{COM} = I_{origin} - m d_{origin}^2 \quad (4)$$

$$I_{cr} = I_{COM} + m d_{cr}^2 \quad (5)$$

, where *d* is defined as the distance from the center of mass to the specified point, *cr* refers to center of rotation and *origin* is the initial position of the corner of the quarter ellipsoid (*z*-axis, Fig. 2). Combining equations 2-5 results in

$$I_{cr} = m\left(\frac{l^2 + h^2}{5} + d_{cr}^2 - d_{origin}^2\right) \quad (6)$$

, where I_{cr} corresponds to the modeled moment of inertia for the observed pitch rotation of the neurocranium. Although the position of the center of rotation can shift during head rotation in fish (e.g. de Lussanet and Muller, 2007), we are forced to use the average center of rotation of the entire phase of head rotation because the spatial resolution of the lateral-view image does not allow a reliable determination of *cr* for smaller time steps. In our case, point *cr* is determined from two video images: one just before, and one just after completion of head rotation. The positions before and after rotation of two anatomical landmarks (e.g. dorsal tip of the snout, eye or opercular) are connected by lines. Next, lines are drawn perpendicular to the midpoint of each of these lines, and their intersection defines *cr* (Fig

2B). Since the latter procedure is only valid if translation is zero, in case of significant forward locomotion it is necessary to align the trunk of the fish (e.g. pelvic and dorsal fins) on the two analyzed images.

According to Newton's second law for rotation, the instantaneous moment required to overcome the effects of inertia $\boldsymbol{M_{nc}}(t)$ is given by

$$\boldsymbol{M_{nc}}(t) = -I_{cr}\ \ddot{\boldsymbol{\alpha}}(t) + \boldsymbol{M_{am}}(t) \qquad (7)$$

, where $\ddot{\boldsymbol{\alpha}}(t)$ is the instantaneous angular acceleration of neurocranial rotation, and $\boldsymbol{M_{am}}(t)$ the added mass moment (i.e. the moment needed to accelerate the volume of water immediately surrounding the neurocranium). Moments resisting the dorsal rotation (= a positive angular velocity according to right-hand rule with the coordinate system of Fig. 2A) are defined as negative.

The moment required to overcome drag force on the quarter-ellipsoid neurocranium, $\boldsymbol{M_{drag}}(t)$, will also be calculated. This drag force results from the flow that moves over the dorsally rotating neurocranium. A certain fraction of this moment is contributing to repositioning of water at the mouth entrance, for example at the snout tip, which can be regarded as part of the generated flow used to capture the prey. However, the other fraction will move water in a direction (e.g. deflecting laterally) that is not useful for prey capture, and could be regarded as a cost in addition to the inertial costs of eq. 7. Because of this ambiguity to classify drag force either as a hydrodynamic cost or benefit to suction feeding, we will discuss $\boldsymbol{M_{drag}}(t)$ as a separate factor. Note, in this respect, that this moment is probably very small (Van Wassenbergh et al. 2005).

Since power equals the scalar product of the moment and angular velocity vectors, the power required to overcome neurocranial rotation inertia $P_{nc(t)}$ and external hydrodynamic resistance is

$$P_{nc(t)} = \boldsymbol{M}_{\boldsymbol{nc}(t)} \cdot \dot{\boldsymbol{\alpha}}_{(t)} \quad (8)$$

, where $\dot{\boldsymbol{\alpha}}_{(t)}$ is the instantaneous angular velocity of neurocranial rotation. Negative values of power from this equation denote a cost of power that needs to be delivered by the muscles.

2.2 CFD estimates of quarter ellipsoid drag and added mass moment coefficients

The moment required to overcome drag forces and acceleration reaction forces (i.e. added mass) exerted on an elevated quarter of a full ellipsoid that rotates about a principal axis are calculated using computational fluid dynamics (CFD) software. To do so, ellipsoids consisting of four quarters of non-uniform rational B-splines (NURBS) surfaces are constructed using VRMesh 5.0 Studio (VirtualGrid, Bellevue City, USA). The length radius of the ellipsoids is always 50 mm, and 49 combinations of the width and height (as defined in Fig. 2A) of 5, 10, 20, 40, 80, 160 and 320 mm were used. NURBS ellipsoids are imported into ANSYS DesignModeler 14.5.7 (Ansys Inc., Canonsburg, USA) to be surrounded by a spherical flow domain of 300 mm for the smaller ellipsoids, and 1000 mm for the ellipsoids with radii of 160 mm or 320 mm. The flow domain was meshed using Ansys Meshing 14.5.7. In the absence of a formal convergence study, a comparison of moment output from a low density (0.17 million cells) and high density mesh (1.1 million cells) with comparable time step scaling showed an underestimation by 7 ± 5 % (mean ± s.d.), indicating that the level of accuracy of the low-density mesh is sufficient considering the explorative nature of this study. In Ansys Fluent 14.5.7, the ellipsoids are subjected to three constant accelerations, representing a situation with slow, medium and high head acceleration for

feeding fish: (1) 5000 ° s^{-2} (time step size = 0.002 s; number of time steps = 120; final velocity = 1200 ° s^{-1}; angle rotated = 144 °), (2) 25000 ° s^{-2} (time step size = 0.0004 s; number of time steps = 120; final velocity = 1200 ° s^{-1}; angle rotated = 28.8 °), and (3) 100000 ° s^{-2} (time step size = 0.0001 s; number of time steps = 120; final velocity = 1200 ° s^{-1}; angle rotated = 7.2 °). Simulations are unsteady, viscous (i.e. full Navier-Stokes equations solved) laminar flow models, where the mesh of the entire flow domain is rotated at constant acceleration with respect to the fixed reference frame. The outer boundary of the sphere is defined as a pressure outlet. The ellipsoid surfaces have no-slip boundary conditions.

The relative contribution of drag (a velocity dependent factor) and added mass (an acceleration dependent factor) are derived from the slope and intercept of least-squares regression fitted to the calculated hydrodynamic moment at a quarter spheroid surface (more specifically the average of the two representative quarters) divided by water density (ρ = 1000 kg m^{-3}) and head length to the fifth power *versus* the square of instantaneous velocity (Fig. 3). We use the average slope of the three accelerations as an estimate of the moment per squared radian s^{-1} (= dimensionless drag moment coefficient C_{M_drag}) and the average of the three y-axis intercepts divided by their respective acceleration as the moment per radian s^{-2} (= dimensionless added mass moment coefficient C_{M_am}). This allows us to calculate the instantaneous external moment on the quarter ellipsoid due to drag by

$$\boldsymbol{M}_{drag(t)} = -C_{M\_drag}\, l^5\, \rho\, \dot{\boldsymbol{\alpha}}_{(t)} \left|\dot{\boldsymbol{\alpha}}_{(t)}\right| \qquad (9)$$

, and the moment due to acceleration of the added mass by

$$\boldsymbol{M}_{am(t)} = -C_{M\_am}\, l^5\, \rho\, \ddot{\boldsymbol{\alpha}}_{(t)} \qquad (10)$$

,where l is the head length of the specimen. The scaling relationships proportional to l^5 are validated by isometrically doubling the size of one of the CFD models. Note that, in contrast

to the inertial term in eq. (7) which can be calculated for any given left-right axis, eq. (9) as well as eq. (10) imply the rotation occurs about an axis through the corner of the quarter ellipsoid (origin in Fig. 2B) for calculating the external hydrodynamic resistance. We are forced to make this assumption to avoid excessive complication of the model. Note also that the flow regime (i.e., the importance of viscous *versus* inertial effects as captured in the Reynolds number) of the presented drag (Table 1) and added mass moment coefficients (Table 2) corresponds to typical speed and sizes ranges of adult fish, and may therefore not be applicable to individuals with a head length considerably smaller or larger than 50 mm.

2.3 Inverse dynamic calculation of suction power

Suction power output can be assessed using the hydrodynamic resistance experienced by the intra-oral mouth-cavity surfaces moving outward while generating the suction flow (Aerts, 1991; Carroll et al., 2006; de Jong et al., 1987; Van Wassenbergh et al., 2005). Consider a given cross-section of the buccal cavity (Fig. 4). The intra-oral curve of this cross-section that borders the buccal cavity can be divided into chord segments of infinitesimal length *dc* (Fig. 4). This cross-sectional chord *dc* will form a surface segment parallel with the *x*-axis by multiplying it with $d\boldsymbol{x}$, a vector running parallel with the *x*-axis. The surface area of this segment is *dc dx*, while the direction of this surface will be given by the surface normal unit vector $\hat{\boldsymbol{s}}$ which we arbitrarily point away from the buccal cavity center. To generate suction, this surface element will move outward (i.e. away from the buccal cavity center) in the cross-sectional plane by a translation of $d\boldsymbol{r}$ (Fig. 4).

Two types of hydrodynamic forces will be exerted on this surface element: pressure forces and shear forces. Pressure forces act normal to the surface, while shear forces are parallel with the surface. As a given movement causing expansion $d\boldsymbol{r}$ per definition will be perpendicular to the surface (e.g. as in a radial expansion of a cylinder, but the same

relationships would also apply to axially expanding surfaces such as the retracting piston crown in a cylinder), only pressure forces need to be accounted for in our inverse dynamic calculation to resolve power (since only force components parallel with the displacement require power). In our model, we assume that the no pressure force is exerted at the non-wetted side of our intra-oral surface element. In this way, only the intra-oral gauge pressure p_g (i.e. measured pressure – hydrostatic pressure) needs to be considered. Previous computational studies have shown that p_g is uniform along a single cross-section (Van Wassenbergh and Aerts, 2009). Although a limited amount of variation along the length of the buccopharyngeal cavity is possible (Lauder, 1983; Van Wassenbergh and Aerts, 2009), we assume that the average pressure, as measured in-vivo somewhere central in the mouth cavity, is applying uniformly over the entire cavity. Pressure force $\boldsymbol{F_p}$ on the surface segment is given by

$$\boldsymbol{F}_{\boldsymbol{p}(t)} = p_{g(t)}\, dc_{(t)}\, dx\, \hat{\boldsymbol{s}} \tag{11}$$

, so that the instantaneous suction power $P_{s(t)}$ required to generate the opposite force ($-\boldsymbol{F}_{\boldsymbol{p}(t)}$) and thereby achieving a dynamic equilibrium is calculated as

$$P_{s(t)} = -p_{g(t)}\ \hat{\boldsymbol{s}} \cdot \frac{d\boldsymbol{r}_{(t)}}{dt}\, dc_{(t)}\, dx \tag{12}.$$

Since the expansive motions are perpendicular to the intra-oral surface, $\hat{\boldsymbol{s}} \cdot d\boldsymbol{r}_{(t)}$ equals the scalar $dr_{(t)}$. Integrated over the entire buccopharyngeal surface area, total instantaneous suction power $Ps_{(t)}$ is

$$P_{s(t)} = -p_{g(t)} \int_{anterior}^{posterior} \oint \frac{dr_{(t)}}{dt}\, dc_{(t)} dx \tag{13}$$

The total instantaneous expansion volume of the buccal cavity $dV_{buccal(t)}$ equals

$$dV_{buccal(t)} = \int_{anterior}^{posterior} \oint dr_{(t)} dc_{(t)} dx \quad (14).$$

Thus, equation 13 can be rewritten as

$$P_{s(t)} = -p_{g(t)} \frac{dV_{buccal(t)}}{dt} \quad (15)$$

This implies that instantaneous suction power can be calculated if the temporal profiles of intra-oral pressure and increase in head volume are known. Note that eq. (15) assumes pressure to be distributed uniformly over the entire buccal cavity surface. Positive numbers of $P_{s(t)}$ require power input from the musculature causing buccal expansion, negative values of $P_{s(t)}$ mean that the buccal surface motion is driven by energy of the water flow relative to the fish.

2.4 Morphology

Three *Micropterus salmoides* specimens (standard lengths 127, 140, and 190 mm) are used to determine the geometry of the model. Neurocranium length (l) is measured as the distance along the centerline of the body from the rostral tip of the premaxilla up to the level of the anteriormost point on the pectoral fin base. The latter point also serve as the location where neurocranium width (w) is measured. Next, dissecting along the frontal plane through the tip of the premaxilla, the neurocranium (*sensu lato*; also including dorsal parts of the suspensoria and opercula) is removed and weighed. Assuming a tissue density of 1000 kg m^{-3}, the neurocranium height (h) is determined so that the calculated mass of the quarter ellipsoid

formed by *l*, *w* and *h* (Fig. 2) matches the measured mass. The data from the three specimens are then averaged and normalized to neurocranium length (*l*). The best-fitting height position of the quarter ellipsoid is determined by overlaying this model with lateral-view photographs of one of the specimens. These morphological input variables are scaled isometrically to the size of the individuals from which the kinematic data were collected.

2.5 Kinematics

Kinematics of four *Micropterus salmoides* individuals feeding on small goldfish suspended by a small wire are analyzed (one strike per individual). The *M. salmoides* individuals are filmed in 200 liter tanks using a high-speed NAC Memrecam Ci digital system (Tokyo, Japan) operating at 500 images s^{-1}. Lateral and ventral views of the feeding events are obtained via a mirror underneath the prey oriented at 45°. Two floodlights (600 W) on either side of the camera illuminate the experimental tank.

Anatomical landmark positions are determined frame-by-frame to calculate gape distance and neurocranium angle. Gape distance is defined as the distance between the tip of the premaxilla and the tip of the dentary. Four landmarks that are approximately evenly distributed along the dorsal contour of the neurocranium on the lateral-view images are used to calculate the angle of the neurocranium with respect to the earth-bound frame of reference. Digitization noise is reduced by applying a low-pass fourth-order zero phase-shift Butterworth filter (cut-off frequency of 40 Hz) to the raw data. Time-derivatives for calculating angular velocities and accelerations of the neurocranium use the difference between one frame before and one frame after a given instant. A center of head rotation is estimated as described earlier (see Fig. 2B) for each of the four feeding sequences. However, we choose to use the centroid of these four coordinates as the rotation center (*cr*) in our model to reduce random uncertainty in the estimation of the individual rotation centers.

The instantaneous volume of the head is determined using the ellipse method (Drost and van den Boogaart, 1986) in which the expanding head volume is approximated by a series of elliptical cylinders, in which the major and minor axis of each ellipse corresponds to the width and height of the head at a certain position along the head's mediosagittal axis. The upper and lower contours of the head of the largemouth bass are digitized frame-by-frame (20 points each) in lateral and ventral view. At the same time, the coordinates of the mediosagittal axis are also digitized. The contour coordinates are recalculated to a new frame of reference moving with the fish. Next, the distance between the left and right contours are extracted at 21 equally spaced intervals along the mediosagittal line between upper jaw tip and a point in between the tips of the opercula. Similar to the procedure outlined for the standard kinematical analysis, digitization noise is reduced using a Butterworth filter algorithm applied to the profiles of length and width versus time. As the volume of head tissues will not change during suction generation, the instantaneous change in external head volume will equal the instantaneous change in the volume of the buccal cavity ($dV_{buccal(t)}$).

2.6 Pressure

As synchronized recordings of buccal pressure and dual-view high-speed videos are not available to us, pressure profiles of *M. salmoides* are derived from the literature. This is possible since previous studies showed that both the timing and magnitude of pressure can be predicted (within a certain range of uncertainty) based on the kinematic profile of mouth opening (i.e. gape). The time at which the peak negative pressure in *M. salmoides* is reached typically occurs midway between the times the gape reaches 20% and 95% of the maximum gape observed during a strike (Day et al., 2007; Higham et al., 2006b). The pressure magnitude then drops to approach zero (i.e. ambient hydrostatic pressure) within 20 ms after the time of peak gape (Day et al., 2007; Higham et al., 2006b). These relationships of buccal

pressure timing with the gape profile of *M. salmoides* are taken into account in the simulated pressure profiles that are used in our model. The magnitude of the pressure peak is derived from the relationship of this pressure (p_g in kPa) with the time to reach peak gape (*TTPG* in ms) published by Higham and co-workers (Higham et al., 2006b):

$$\log p_g = -0.75 \log TTPG + 1.6 \qquad (16).$$

To cover the 95% prediction interval of this observed relationship, additional model simulations are performed with the intercept (constant 1.6) increased by 0.47 to obtain the upper 95% prediction limit for p_g and decreased by 0.47 to obtain the lower 95% prediction limit.

3. Results

3.1 Model geometry

The measurements of three *M. salmoides* individuals (head length (l) = 48 ± 10 mm; mean ± s.d.) show a mean head width of 0.53 ± 0.07 l. The calculated height to achieve a balance between the measured neurocranium mass and that of the quarter ellipsoid model is 0.34 ± 0.07 l (Fig. 4). Using cubic spline interpolation with the data in Tables 1 and 2 reveals a drag moment coefficient of -0.0018 and an added mass coefficient of 0.0081, respectively. The selected alignment of the quarter ellipsoid with respect to the head is shown in Figure 4. A mean center of rotation (white cross in Fig. 5) is obtained from the positions of the center of rotation determined separately on each of the four prey-capture videos (white spheres in Fig. 5). The head length of the individuals (numbered 1 to 4) from these four videos is respectively 5.61, 5.88, 6.09, and 7.12 cm. These head lengths result into neurocranium quarter ellipsoid model masses of, respectively, 16.3, 18.8, 20.9, and 33.4 g (i.e., identical to the measured masses), and pitching moments of inertia about the mean center of rotation of,

respectively, 0.95, 1.20, 1.43, and 3.11 x 10^{-5} kg m^2 (83% of the moments of inertia about the corner of the quarter ellipsoid).

3.2 Kinematic input and simulated pressures

Time zero is set as the start of mouth opening. Dorsal rotation of the neurocranium lasts up to 48 ± 12 ms, of which it accelerates during the first 31 ± 10 ms (Fig. 6A,B). The time of peak neurocranium acceleration (20 ± 9 ms) precedes the estimated time of peak suction pressure by 6 ± 3 ms (Fig. 6B,D). The relatively low correlation coefficient of pressure magnitude in function of time to peak gape for *M. salmoides* (Higham et al., 2006b; r^2 = 0.29), results in a relatively large 95% prediction interval for peak pressure (between -12 ± 2 kPa and -1.4 ± 0.2 kPa; Fig. 6D). The rate of volume increase calculated by the ellipse modelling procedure shows a very consistent pattern, with a negligible speed during the approximate initial 13 ± 6 ms, followed by a rapid increase in speed up to a maximum at 40 ± 10 ms.

3.3 Model output

The peak moment to overcome the effects of inertia when rotating the neurocranium (M_{nc}, eq. (7)) is -0.018 ± 0.017 N m, and is reached at 19 ± 8 ms (Fig.6E). The acceleration of the neurocranial mass is the dominant factor in this variable, being responsible for about 68% of this moment. The moment due to added mass (about 32% of M_{nc}) is significantly smaller. The overall moment M_{nc} contributed to a peak power cost (P_{nc}) of -0.15 ± 0.16 W (Fig. 6F) reached at 22 ± 9 ms. The mean work in the interval of negative P_{nc} is -0.0019 ± 0.0023 J, which equals the kinetic energy of the rotating neurocranium (and added mass) at the peak observed velocity. Because of the negative drag moment coefficient for the leading quartile of the rotating ellipsoid matching the shape of *M. salmoides* neurocranium (due to dominant negative pressures at its lateral sides), a moment to overcome steady-state drag on the roof of

the neurocranium was not required: this flow resulted in a negligibly small moment (median 0.03% of M_{nc}) assisting dorsal rotation of the neurocranium.

Peak suction power is generated at a later instant than peak P_{nc}, namely at 31 ± 16 ms (Fig. 6G). Peak suction power magnitude, on average 6 ± 4 W (upper 95% pressure limit = 19 ± 13 W, lower 95% pressure limit = 2.2 ± 1.5 W) is consistently higher than peak P_{nc}, on average 0.15 ± 0.16 W. The ratio of peak P_{nc} over peak P_s is 0.019 ± 0.009 (upper 95% pressure limit = 0.007 ± 0.003, lower 95% pressure limit = 0.057 ± 0.026). At the time of peak P_{nc}, the ratio of P_{nc} over P_s is 0.040 ± 0.019 (upper 95% pressure limit = 0.014 ± 0.006, lower 95% pressure limit = 0.11 ± 0.05). The total work of generating suction is 0.11 ± 0.08 J (upper 95% pressure limit = 0.3 ± 0.2 J, lower 95% pressure limit = 0.04 ± 0.03 J). The ratio of the mechanical energy cost of neurocranial rotation during the interval of negative P_{nc} over the total suction work is 0.015 ± 0.009 (upper 95% pressure limit = 0.005 ± 0.003, lower 95% pressure limit = 0.045 ± 0.027)

4. Discussion and conclusion

We found that the inertial costs of rotating the neurocranium have a negligible impact on suction performance in largemouth bass, a generalized percomorph suction feeder. We estimated the loss not to exceed 4.0% of the generated suction power throughout the feeding sequence. In the worst case scenario for the bass, when focussing on the time at which this cost was maximal and performing the simulations with the lowest possible pressure magnitudes, the loss in power was 11% of the generated suction power. Yet, even in this worst case scenario, the energetic cost in neurocranial acceleration was only about 4.5% of the delivered suction work. However, an equally plausible scenario, using actual pressures approaching the upper limit observed in previous studies (Higham et al., 2006b; Svanbäck et

al., 2002), predicted power and work for cranial rotation are less than 1.5% of suction power and work.

Independent of which scenario was followed, we can conclude that the head expansion system involving neurocranial dorsorotation efficiently transfers muscle power to drawing water into the mouth in our model species. Given the considerably smaller mass of the anatomical elements bordering the lateral and ventral side of the buccal cavity compared to the neurocranium, it can be expected that the total inertial cost of head expansion will be less than twice the calculated values presented here for the neurocranial rotation. A previous study on the catfish *Clarias gariepinus* estimated this total inertial cost to be about 10% (Van Wassenbergh et al., 2005). However, a later computational study showed that the equations used in that study are likely to underestimate intra-oral pressure by a factor of 2 (Van Wassenbergh and Aerts, 2009), which would imply a total inertial cost of about 5% for *C. gariepinus*. Because of the (on-average) absence of neurocranial rotation in *C. gariepinus*, we *a priori* expected the inertial costs to be higher for the largemouth bass due to its considerable neurocranial rotation. Our data showed that this is not the case, as the total inertial costs in *M. salmoides* are likely to be of similar or even lower magnitude than this 5% estimate for *C. gariepinus*.

The kinetic energy put into rotational acceleration of the neurocranium may be converted to suction work when the neurocranium decelerates. The timing of the calculated profiles of suction feeding dynamics show neurocranial deceleration (movement energy being attenuated) overlapping the phase when suction is still being generated (Fig. 6B,G). As the dorsal rotation of the roof of the buccal cavity contributes to buccal expansion, the deceleration of this dorsal rotation of the neurocranium may thus contribute to powering suction. This can similarly be viewed as the neurocranium being decelerated by the negative

buccal pressures, to which its own movement contribute, exerted at its ventral surface. Work invested by the feeding musculature into acceleration of musculoskeletal elements involved in buccal expansion early in the suction act may thus contribute to suction at a later instant when these elements decelerate. The idea of conversion of kinematic energy of cranial rotation to suction has been proposed previously for syngnathid fishes (de Lussanet and Muller, 2007). Although the mechanism and timing of suction generation relative to cranial rotation is highly modified in syngnathids (Van Wassenbergh et al., 2013, 2014), the same energy conversion principle may thus apply during suction feeding by *M. salmoides*. This could further reduce or even erase the already very low energetic cost to suction performance due to neurocranial acceleration.

Our results support one of the assumptions of several recent publications that link the size of the epaxial muscles to suction performance (so-called suction index) in species showing variation in head size and shape (Carroll et al., 2004; Collar and Wainwright, 2006; Holzman et al., 2012a, 2012b). This assumption was that the proportion of muscle power that goes into acceleration of cranial elements is overall negligible or similar between species, so that the inertial properties of the head have no influence on the suction index. Our results suggest that this is a valid assumption for species that do not differ too drastically from the largemouth bass in cranial morphology or behaviour.

It can be concluded that the relatively low cost of neurocranial rotation explains why this motion is not avoided in many suction-feeding species (Gibb and Ferry-Graham, 2005; Muller, 1987). It also allows the post-cranial muscles inserting dorsally of the cranio-vertebral articulation to be recruited in a mechanically efficient way to power suction (Camp and Brainerd, 2014). This result also indirectly implies that size, shape and mass distribution of the neurocranium is not likely to be evolutionary constrained by suction performance (but

see pipefish and seahorses for exceptions; de Lussanet and Muller, 2007; Roos et al., 2010), which perhaps contributed to the extensive diversity of suction feeding fishes.

Acknowledgements

This work was conducted as a part of the Suction Feeding Biomechanics Working Group at the National Institute for Mathematical and Biological Synthesis, sponsored by the National Science Foundation through NSF Award #DBI-1300426, with additional support from The University of Tennessee, Knoxville. CFD software and hardware was funded by grants from the Fund for Scientific Research Flanders (FWO Grant 1.5.160.08.N.00) and the University of Antwerp (BOF/KP 24346). Further support was provided by FWO grant G014911N to SVW. We thank the two reviewers for helping us to improve our article.

References

Aerts, P., 1991. Hyoid morphology and movements relative to abducting forces during feeding in *Astatotilapia elegans* (Teleostei: Cichlidae). J. Morphol. 208:323-345. doi: 10.1002/jmor.1052080308

Camp, A., Brainerd, E., 2014. Role of axial muscles in powering mouth expansion during suction feeding in Largemouth Bass. J. Exp. Biol. 217, 1333-1345. doi:10.1242/jeb.095810

Carroll, A.M., Wainwright, P.C., 2006. Muscle function and power output during suction feeding in largemouth bass, *Micropterus salmoides*. Comp. Biochem. Physiol. A 143, 389-399. doi: 10.1016/j.cbpa.2005.12.022

Carroll, A.M., Wainwright, P.C., 2009. Energetic limitations on suction feeding performance in Centrarchidae. J. Exp. Biol. 212, 3241-3251. doi:10.1242/jeb.033092

1 Carroll, A.M., Wainwright, P.C., Huskey, S.H., Collar, D.C., Turingan, R.G., 2004.
2 Morphology predicts suction feeding performance in centrarchid fishes. J. Exp. Biol. 207,
3 3873-3881. doi:10.1242/jeb.01227

4 Collar, D.C., Wainwright, P.C., 2006. Discordance between morphological and mechanical
5 diversity in the feeding mechanism of centrarchid fishes. Evolution 60: 2575-2584.

6 Coughlin, D.J., Carroll, A.M., 2006. In vitro estimates of power output by epaxial muscle
7 during feeding in largemouth bass. Comp. Biochem. Phys. A 145, 533–539.
8 doi:10.1016/j.cbpa.2006.08.026

9 Day, S.W., Higham, T.E., Wainwright, P.C. 2007. Time resolved measurements of the flow
10 generated by suction feeding fish. Exp. Fluids 43, 713-724. doi:10.1007/s00348-007-0405-0

11 de Jong, M.C., Sparenberg, J.A., de Vries, J., 1987. Some aspects of the hydrodynamics of
12 suction feeding in fish. Fluid. Dyn. Res. 2, 87-112. doi: 10.1016/0169-5983(87)90021-9

13 de Lussanet, M.H.C., Muller, M., 2007. The smaller your mouth, the longer your snout:
14 predicting the snout length of *Syngnathus acus*, *Centriscus scutatus* and other pipette feeders.
15 J. R. Soc. Interface 4, 561-573. doi:10.1098/rsif.2006.0201

16 De Visser, J., Barel, C.D.N., 1996. Architectonic constraints on the hyoid's optimal starting
17 position for suction feeding of fish. J. Morphol. 228, 1-18. doi: 10.1002/(SICI)1097-
18 4687(199604)228:1<1::AID-JMOR1>3.0.CO;2-B

19 Drost M.R., van den Boogaart, J.G.M., 1986. A simple method for measuring the changing
20 volume of small biological objects, illustrated by studies of suction feeding by fish larvae and
21 of shrinkage due to histological fixation. J. Zool., Lond. 209, 239–249. doi:10.1111/j.1469-
22 7998.1986.tb03579.x

1 Gibb, A.C., Ferry-Graham, L.A., 2005. Cranial movements during suction feeding in teleost
2 fishes: are they modified to enhance suction production? Zoology 108,141-153.
3 doi:10.1016/j.zool.2005.03.004

4 Gregory, W.K., 2002. Fish skulls: a study of the evolution of natural mechanisms. Originally
5 published in the transactions of the American Philosophical Society, Volume Twenty-three,
6 part two. Krieger Publishing Company, Malabar, USA.

7 Higham, T.E., Day, S.W., Wainwright, P.C., 2006a. Multidimensional analysis of suction
8 feeding performance in fishes: fluid speed, acceleration, strike accuracy and the ingested
9 volume of water. J. Exp. Biol. 209, 2713-2725. doi:10.1242/jeb.02315

10 Higham, T.E., Day, S.W., Wainwright, P.C., 2006b. The pressures of suction feeding: the
11 relation between buccal pressure and induced fluid speed in centrarchid fishes. J. Exp. Biol.
12 209, 3281-3287. doi:10.1242/jeb.02383

13 Holzman, R., Day, S.W., Wainwright, P.C., 2007. Timing is everything: coordination of
14 strike kinematics affects the forces exerted by suction feeding fish on attached prey. J. Exp.
15 Biol. 210, 3328-3336. doi:10.1242/jeb.008292

16 Holzman, R., Collar, D.C., Mehta, R.S., Wainwright, P.C., 2012b. An integrative approach to
17 elucidate suction feeding performance. J. Exp. Biol. 215, 1-13. doi:10.1242/jeb.057851

18 Holzman, R., Collar, D.C., Price, S.A., Hulsey, C.D., Thomson R.C., Wainwright, P.C.,
19 2012a. Biomechanical trade-offs bias rates of evolution in the feeding apparatus of fishes.
20 Proc. R. Soc. B. 279, 1287-1292. doi:10.1098/rspb.2011.1838

21 Landau, L.D., Lifshitz, E.M., 1976. Mechanics, Course of Theoretical Physics Volume 1
22 (Third Edition). Elsevier Butterworth-Heinemann, Oxford.

1 Lauder, G.V., Schaffer, H.B., 1993. Design of feeding systems in aquatic vertebrates : major
2 patterns and their evolutionary interpretations, in: Hanken, J., Hall, B.K. (Eds.), The Skull
3 (Vol.3), functional and evolutionary mechanisms. The University of Chicago Press, Chicago
4 & London, pp. 113-149.

5 Lauder, G.V., 1983. Prey capture hydrodynamics in fishes: experimental tests of two models.
6 J. Exp. Biol. 104, 1-13.

7 Muller, M., 1987. Optimization principles applied to the mechanism of neurocranial levation
8 and mouth bottom depression in bony fishes (Halecostomi). J. Theor. Biol. 126, 343-368.

9 Muller, M., 1989. A quantitative theory of expected volume changes of the mouth during
10 feeding in teleost fishes. J. Zool., Lond. 217, 639-662. doi:10.1111/j.1469-
11 7998.1989.tb02515.x

12 Osse, J.W.M., 1968. Functional morphology of the head of the perch (*Perca Fluviatilis* L.):
13 an electromyographic study. Neth. J. Zool. 19, 289-392. doi:10.1163/002829669X00134

14 Roos, G., Van Wassenbergh, S., Herrel, A., Adriaens, D., Aerts, P., 2010. Snout allometry in
15 seahorses: insights on optimisation of pivot feeding performance during ontogeny. J. Exp.
16 Biol. 213, 2184-2193. doi:10.1242/jeb.040972

17 Skorczewski, T., Cheer, A., Cheung, S., Wainwright, P.C., 2010. Use of computational fluid
18 dynamics to study forces on prey by aquatic suction feeders. J. R. Soc. Interface. 7, 475-484.
19 doi:10.1098/rsif.2009.0218

20 Svanbäck, R., Wainwright, P.C., Ferry-Graham, L.A., 2002. Linking cranial kinematics,
21 buccal pressure and suction feeding performance in largemouth bass. Physiol. Biochem.
22 Zool. 75, 532-543. doi:10.1086/344495

Thys, T., 1997. Spatial variation in epaxial muscle activity during prey strike in largemouth bass (*Micropterus salmoides*). J. Exp. Biol. 200, 3021-3031.

van Leeuwen, J.L., 1984. A quantitative study of flow in prey capture by rainbow trout, with general considerations of the actinopterygian feeding mechanism. Trans. Zool. Soc. Lond. 37, 171-227. doi:10.1111/j.1096-3642.1984.tb00070.x

Van Wassenbergh, S.**,** Aerts, P., Herrel, A., 2005. Scaling of suction-feeding kinematics and dynamics in the African catfish, *Clarias gariepinus*. J. Exp. Biol. 208, 2103-2114. doi:10.1242/jeb.01603

Van Wassenbergh, S., Herrel, A., Adriaens, D., Aerts, P., 2007a. No trade-off between biting and suction feeding performance in clariid catfishes. J. Exp. Biol. 210, 27-36. doi: 10.1242/jeb.02619

Van Wassenbergh, S., Herrel, A., James, R.S., Aerts, P., 2007b. Scaling of contractile properties of catfish feeding muscles. J. Exp. Biol. 210, 1183–1193. doi:10.1242/jeb.000109

Van Wassenbergh, S., Aerts, P., 2009. Aquatic suction feeding dynamics: insights from computational modelling. J. R. Soc. Interface. 6, 149-158. doi:10.1098/rsif.2008.0311

Van Wassenbergh, S., Leysen, H., Adriaens, D., Aerts, P., 2013. Mechanics of snout expansion in suction feeding seahorses: musculoskeletal force transmission. J. Exp. Biol. 216, 407-417. doi:10.1242/jeb.074658

Van Wassenbergh, S., Dries, B., Herrel, A., 2014. New insights into muscle function during pivot feeding in seahorses. PLoS ONE 9(10): e109068. doi:10.1371/journal.pone.0109068

Wainwright, P.C., Day, S.W., 2007. The forces exerted by aquatic suction feeders on their prey. J. R. Soc. Interface 4, 553-560. doi:10.1098/rsif.2006.0197

Tables

Table 1: Drag moment coefficients of a quarter of an ellipsoid in function of width and height to be used with eq. (9).

C_{M_drag}		**width aspect ratio (*w*/*l*)**						
		0.1	**0.2**	**0.4**	**0.8**	**1.6**	**3.2**	**6.4**
height aspect ratio (*h*/*l*)	**0.1**	0.0002	-0.0015	-0.0037	-0.0007	0.0191	0.0449	0.0739
	0.2	0.0002	-0.0006	-0.0025	-0.0073	-0.0128	-0.0210	-0.0666
	0.4	0.0007	0.0004	-0.0003	-0.0017	-0.0055	-0.0132	-0.0290
	0.8	0.0018	0.0014	0.0013	0.0019	0.0016	0.0032	0.0070
	1.6	0.0082	0.0072	0.0078	0.0155	0.0467	0.1346	0.3468
	3.2	0.0696	0.0832	0.1779	0.5880	2.1855	6.6637	18.026
	6.4	0.8385	1.4974	4.3943	14.304	56.911	183.01	612.14

See Fig. 2A for definitions of head length (*l*), width (*w*) and height (*h*)

Table 2: Added mass moment coefficients of a quarter of an ellipsoid in function of width and height to be used with eq. (10).

C_{M_am}		**width aspect ratio (*w*/*l*)**						
		0.1	**0.2**	**0.4**	**0.8**	**1.6**	**3.2**	**6.4**
height aspect ratio (*h*/*l*)	**0.1**	0.0006	0.0020	0.0068	0.0215	0.0604	0.1519	0.3420
	0.2	0.0006	0.0019	0.0061	0.0195	0.0525	0.1245	0.2736
	0.4	0.0006	0.0014	0.0044	0.0142	0.0410	0.0996	0.2161
	0.8	0.0010	0.0008	0.0013	0.0027	0.0074	0.0184	0.0411
	1.6	0.0043	0.0051	0.0109	0.0325	0.1037	0.2928	0.7083
	3.2	0.0347	0.0650	0.1961	0.6991	2.4320	7.7295	20.467
	6.4	0.3143	0.5929	1.9016	7.1212	25.039	83.511	210.56

See Fig. 2A for definitions of head length (*l*), width (*w*) and height (*h*)

Figure legends

Fig. 1 Components and motions responsible for the main power input for suction feeding. Schematic illustrations at the start (A) and at maximum head expansion (B) are given. Drawings are based on video images (Svanbäck et al., 2002) and skeletal drawings (Gregory, 2002).

Fig. 2 Geometry of the quarter ellipsoid model used for inverse dynamics calculation of the power required to accelerate the neurocranium. The oblique frontal view (A) shows the neurocranium dimensions used in the model (l = length, w = width , h = height), while the lateral view (B) shows the coordinate system's origin at the *origin* point, the centre of mass (COM) position, and illustrates the procedure used to determine the centre of rotation (*cr*) though the intersection of the midperpendiculars of lines p1-p1' and p2-p2' (the accent denotes the position after neurocranial rotation).

Fig. 3 CFD model geometry and example of hydrodynamic moments of a rotating ellipsoid. Data is shown for an ellipsoid with radii of 50 mm long, 80 high and 40 mm wide at three constant accelerations. CFD data was sampled once every 10 time steps for ellipsoid quarters 1 and 3 (q1, q3). Regressions used to derive the coefficients of drag moment and added mass moment, and the final single equation model is illustrated. See 2.2 for further information.

Fig. 4 Outline of the model input for deriving the equations to calculate suction power output. Input variables are the pressure forces (gauge pressure p_g) and expansive motion of the buccopharyngeal cavity surfaces ($d\boldsymbol{r}$). Cross-sectional curve segments dc and anterior-posterior increments dx form the surface increment which has the unit normal vector $\hat{\boldsymbol{s}}$.

Fig. 5 Geometry of the largemouth bass model. The height (h) and width (w) of the relative to head length (l) and position of the quarter ellipsoid model of the neurocranium as well as

the measured centers of head rotation (open spheres) and their centroid (white cross) are illustrated. Scale bar, 20 mm.

Fig. 6 Kinematic input and model output of four prey-capture events by largemouth bass. Panels show the kinematic input of neurocranial rotation (A-B; positive = snout moving dorsally) and rate of head volume change (C; positive = expansion), simulated pressure profiles (with 95% prediction interval range as grey curves) (D; eq. (14)), the calculated neurocranium moment (E; eq. (7); negative = resisting the dorsal rotation) and power (F, eq. (8); negative = power required from action of muscles and tendons) to overcome effects of head mass inertia and hydrodynamic forces exerted at the external surface, suction power output (G, eq. (13)).

Figure 1

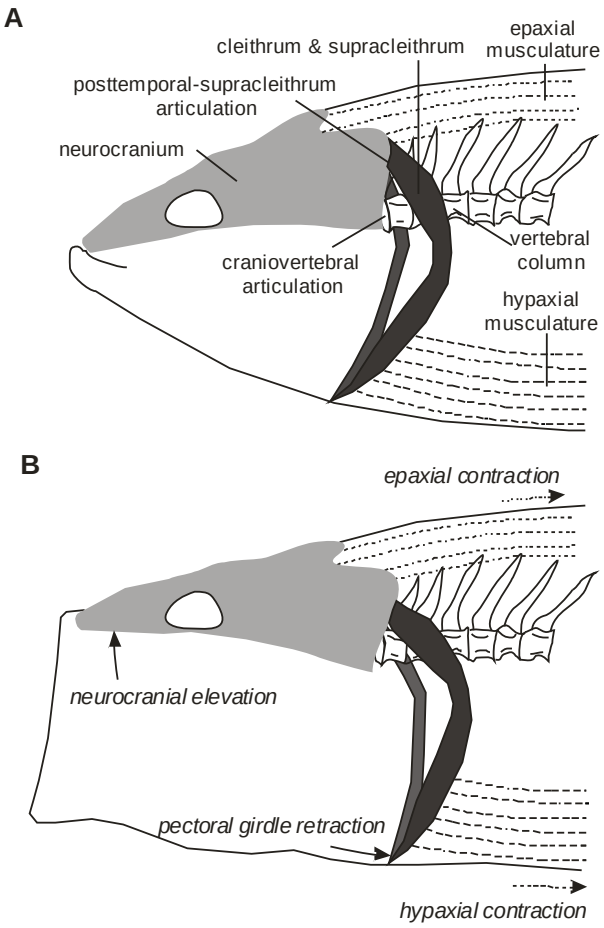
A
cleithrum & supracleithrum
epaxial musculature
posttemporal-supracleithrum articulation
neurocranium
craniovertebral articulation
vertebral column
hypaxial musculature
B
epaxial contraction
neurocranial elevation
pectoral girdle retraction
hypaxial contraction

Figure 2

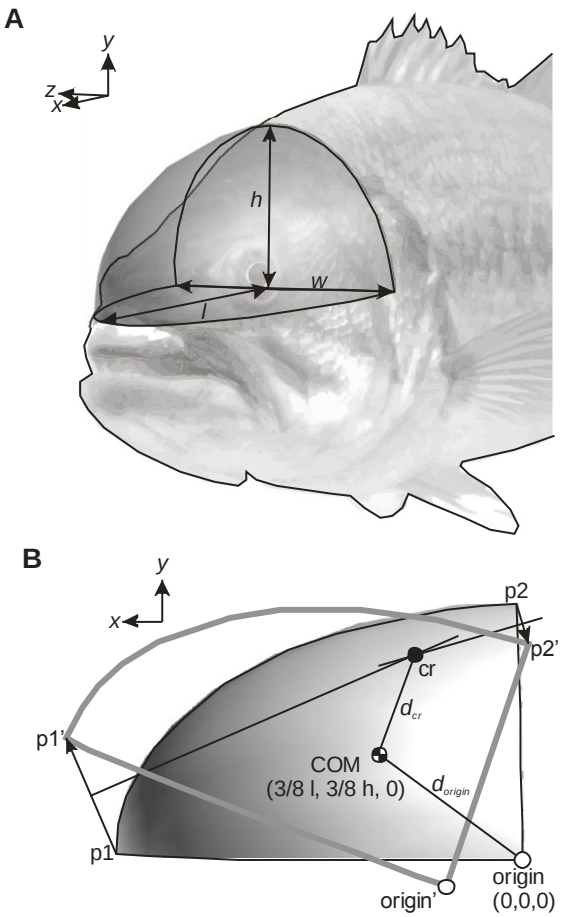
A
y
z
x
h
w
l
B
y
x
p2
p2'
cr
d_{cr}
p1'
COM
(3/8 l, 3/8 h, 0)
d_{origin}
p1
origin'
origin
(0,0,0)

Figure 3

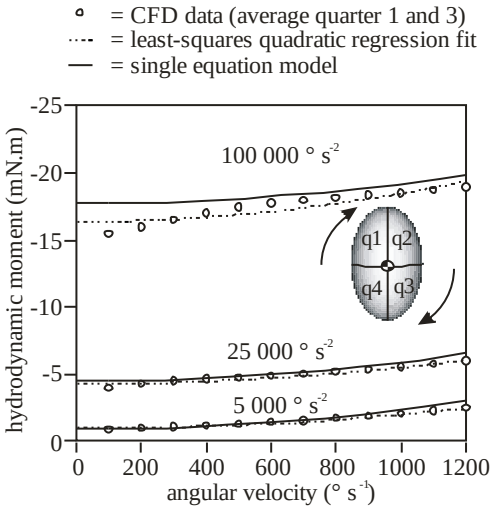

Figure 4

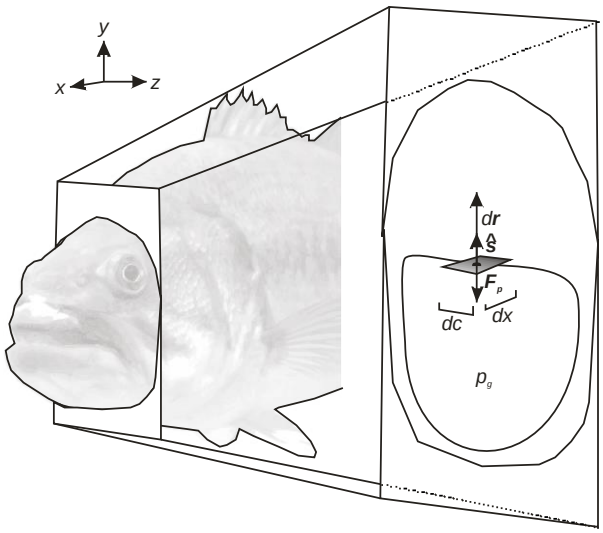

Figure 5

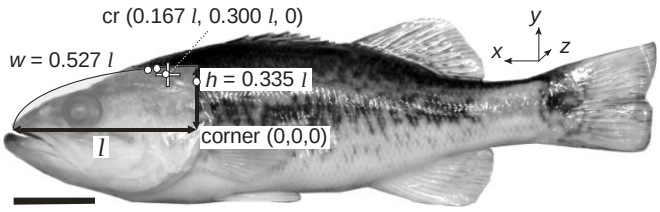

Figure 6

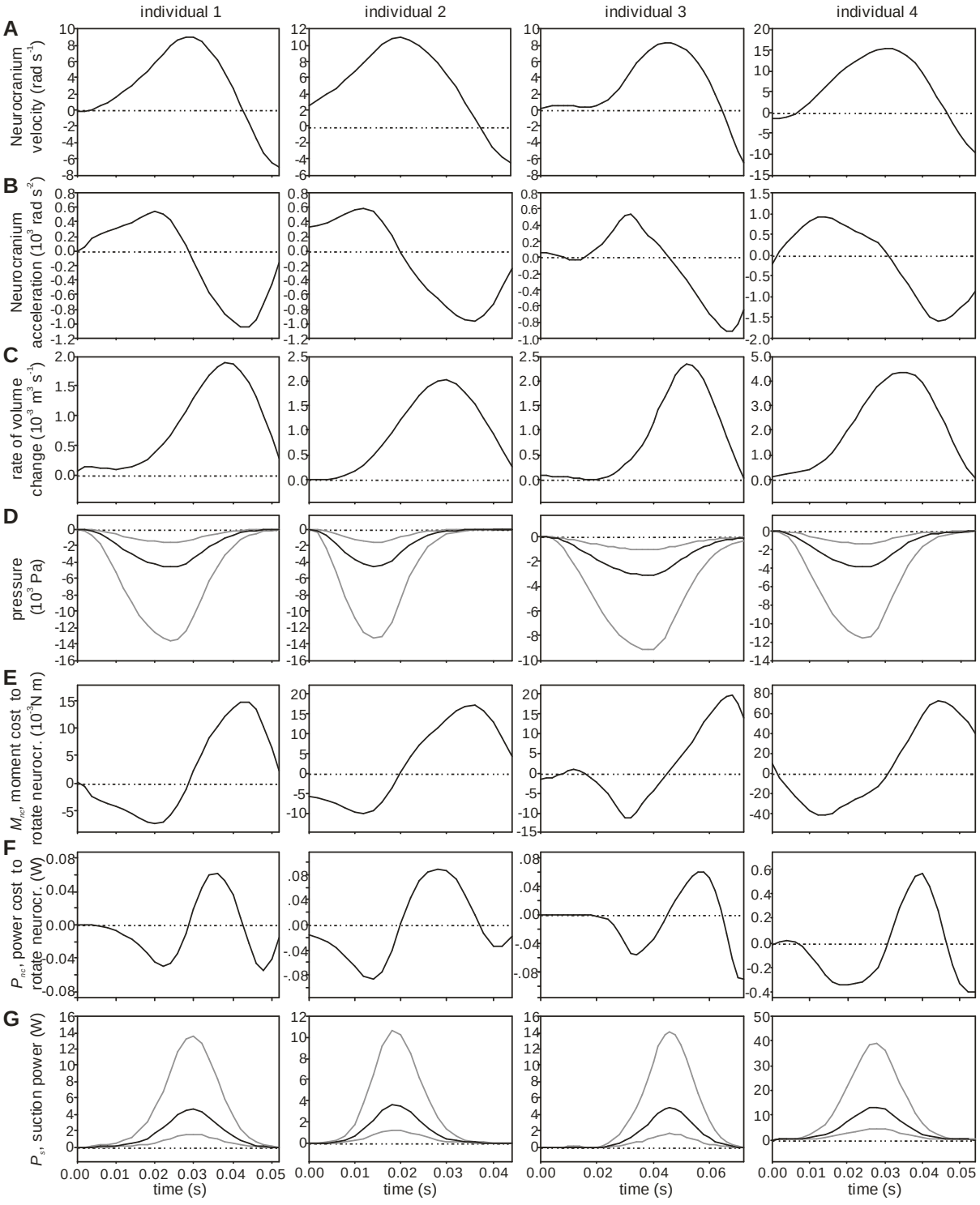
individual 1
individual 2
individual 3
individual 4
A
Neurocranium velocity (rad s-1)
B
Neurocranium acceleration (10-3 rad s-2)
C
rate of volume change (10-3 m3 s-1)
D
pressure (10-3 Pa)
E
Mnc, moment cost to rotate neurocr. (10-3 N m)
F
Pnc, power cost to rotate neurocr. (W)
G
Ps, suction power (W)
time (s)